Q. J. R. Meteorol. Soc. (2005), **131**, pp. 2937–2955 doi: 10.1256/qj.04.122

The effects of wind shear on cirrus: A large-eddy model and radar case-study

By J. H. MARSHAM* and S. DOBBIE
University of Leeds, UK

(Received 6 August 2004; revised 16 March 2005)

SUMMARY

Wind shear is an almost ubiquitous feature of the troposphere at cirrus altitudes, but there have been few studies focused on investigating its effects on cirrus clouds. In this study we consider a case of strongly sheared frontal ice cloud, which was observed by the Chilbolton radar. This was simulated using the Met Office large-eddy model (LEM), which included a fully integrated radiation code. It is well known that there can be significant variations between results from different cirrus models, which makes a comparison of the simulations with observations important. So, radar observations of ice water content (IWC) were simulated directly within the framework of the LEM, and true and simulated IWC observations were compared, as well as their Fourier transforms and probability density functions (p.d.f.s). This showed that the LEM was capturing reasonably well the horizontally averaged IWC profile, and also at upper levels the variability in the IWC field, at scales of less than approximately 14 km. At lower levels the IWC field was too homogeneous.

Varying the shear within the LEM simulations showed that shear had little effect on the mean IWC profile, but it increased the mixing and so the homogeneity of the IWC field. P.d.f.s of IWC derived from the simulated radar data compared well with observed p.d.f.s, except that the largest IWCs were not captured and there was too little variance at lower levels. Comparing p.d.f.s of IWC and total water for runs with and without shear clearly showed the effects of shear-induced mixing. LEM results also showed that the variation of the correlation of IWC with vertical separation is shear dependent and initially linear, with or without shear. In this case, shear had little effect on the top-of-atmosphere and surface fluxes, or the within-cloud heating rate profile, but this would be significantly different for a more patchy cloud.

A modified case-study, which allowed Kelvin–Helmholtz wave breaking, showed that wave breaking can significantly affect the microphysical processes, by increasing nucleation, deposition and sublimation rates. Wave breaking can occur in thin layers of limited horizontal extent, which would not be resolved by a global model. These effects were most significant when there was no large-scale uplift and the vertical velocities from the wave breaking formed a cirrus cloud which did not otherwise occur.

KEYWORDS: Cloud Decorrelation Kelvin–Helmholtz wave breaking

1. INTRODUCTION

Cloud-resolving models (CRMs) are invaluable tools for understanding cloud processes. However, for cirrus clouds there are few direct comparisons of models with observations, even though model intercomparisons show a wide range of results (Starr *et al.* 2000). In this paper, shear effects are investigated by simulating a case of cirrus clouds observed by the Chilbolton radar (Hogan and Illingworth 2003) with the UK Met Office large-eddy model (LEM). Cirrus clouds often form in regions of high wind shear (either at fronts, near jet streams, or in convective outflow), but there has been limited research on the effects of the shear on the cirrus clouds. In this study, the LEM allows the effects of varying the shear to be investigated, whilst comparing real and simulated radar observations ensures that the ice water content (IWC) field in the LEM is realistic.

Wind shear can spread clouds horizontally, by advecting air at different levels at different speeds, and increase turbulence, particularly if the shear is strong enough to initiate Kelvin–Helmholtz wave breaking (Turner 1973). These processes in turn couple with the microphysics and radiative heating rates, and so affect cloud dynamics. To improve cirrus parametrizations, we must first understand the key factors influencing cirrus and so the factors needed in a parametrization for a larger-scale model (if one is possible). Improved parametrizations should lead to a better understanding of

* Corresponding author: Environment, School of Earth and Environment, University of Leeds, Leeds LS2 9JT, UK. e-mail: jmarsham@env-leeds.ac.uk

© Royal Meteorological Society, 2005.

the effects of cirrus on climate, which are currently not well understood (Lynch *et al.* 2002).

Previous observational studies have shown the importance of wind shear in generating turbulence and inhomogeneity in cirrus clouds (Dmitriev *et al.* 1984; Quante and Brown 1992; Smith and Jonas 1996). Turbulence tended to be patchy and anisotropic, because of the atmospheric stability. Smith and Jonas (1996) analysed data from three cirrus clouds over the UK. These clouds were 3 to 4 km thick and had IWC between 0.1 and 0.4 gm^{-3} (i.e. similar to the case-study presented in this paper, though wind shears tended to be higher in our case). Turbulent kinetic energy (TKE) production from breaking Kelvin–Helmholtz waves was noted in all three cases, as well as gravity waves. In this paper we modify our original case-study in order to investigate the effects of Kelvin–Helmholtz wave breaking. This case is a less stable version of the observed case, so the modelled fields are not compared with observations. However, the success of the LEM in reproducing the observations in the first case-study shows that the LEM is providing a reasonable simulation of sheared frontal cirrus.

Shear effects have not been thoroughly investigated in previous cirrus modelling studies. Many simulations have considered idealized atmospheres, with zero shear (Gu and Liou 2000; Starr *et al.* 2000; Dobbie and Jonas 2001; Liu *et al.* 2003). These simulations used horizontally homogeneous cloud-free initial states, with small random perturbations added to generate inhomogeneity. Cooling, or large-scale uplift, was applied to form the cloud. Observationally based simulations of cirrus have used TOGA-COARE* observations (Brown and Heymsfield 2001), ARM† data (Benedetti and Stephens 2001) and FIRE‡ II data (Cheng *et al.* 2001). The latter observed shear-induced gravity waves in one case. These observationally based simulations have tended to force the CRM boundaries with mesoscale models and have used horizontal resolutions between 150 m and 2 km, i.e. some are large-eddy-resolving and some are only cloud-resolving. Simulations in this paper are initialized by cooling the LEM to an observed profile to simulate the observed frontal uplift, thus avoiding the need for mesoscale simulations. Radar data were simulated using the LEM and the simulated radar data were compared with observations from the Chilbolton radar (from Hogan and Illingworth 2003), to ensure that the modelled IWC field was realistic.

CRM experiments allow investigations of the sub-grid parameters used in the representations of clouds in global circulation models (GCMs), but since there are significant differences between CRMs (Starr *et al.* 2000), studies should ideally be based on, and compared with, observational results. GCM cloud schemes are gradually becoming more complex. Firstly, there is a move towards statistical prognostic schemes. These use the probability density functions (p.d.f.s) of variables (e.g. total water content) to account for the sub-grid variability in those variables (Tompkins 2002; Wilson and Gregory 2003). Secondly, attempts are being made to account for the sub-grid variations in cloud's optical depth in radiative transfer schemes (Barker 1996). It is known that the plane-parallel-homogeneous (PPH) assumption used in GCMs, which ignores inhomogeneities within cirrus, introduces bias in radiative fluxes (Liou and Rao 1996; Larson *et al.* 2001; Buschmann *et al.* 2002). Cloud overlap assumptions are also gradually becoming more complex (Hogan and Illingworth 2000; Li *et al.* 2005) and Hogan and Illingworth (2003) derived the vertical decorrelation of the IWC field from Chilbolton radar data. The use of the LEM allows p.d.f.s of unobserved parameters

* Coupled Ocean–Atmosphere Experiment of the Tropical Ocean–Global Atmosphere project.

† Atmospheric Radiation Measurement project.

‡ First Regional Experiment of the International Satellite Cloud Climatology project.

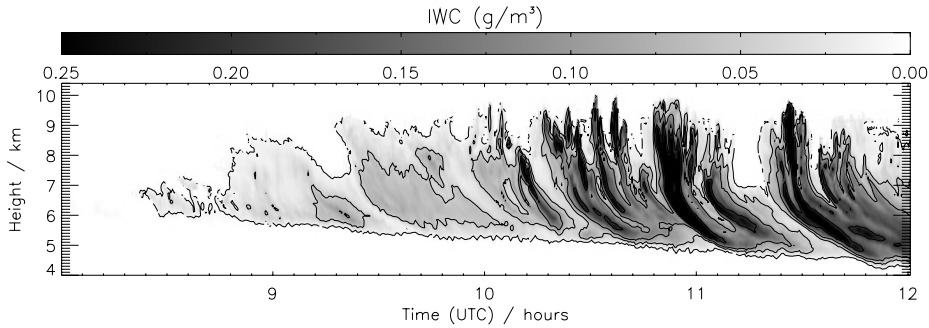

Figure 1. Radar retrievals of ice water content (IWC) from the Chilbolton 94 GHz radar on 27 December 1999 (Hogan and Illingworth 2003). Contours are at 0.01, 0.05, 0.1 and 0.2 g m^{-3}. Errors in IWC of less than a factor of two are expected. Note that the aspect ratio used is misleading (one hour actually corresponds to approximately 180 km at an altitude of 8 km).

(such as the total water content, used by Tompkins (2002)), and also the effects of varying the shear, to be investigated.

Section 2 describes the case-study of sheared cirrus used. Section 3 describes the Met Office LEM and the model initialization, and makes initial comparisons between the model and the radar observations. Section 4 discusses the effect of the shear on the cirrus in the LEM simulations of the case-study, and sections 4(a) and (b) highlight the effects on p.d.f.s and the vertical decorrelations of IWC. Section 4(c) describes the radiative processes. A second modified case-study, with more extensive wave breaking, is investigated in section 5, which includes a case where the cloud is formed only by wave breaking, rather than by cooling to simulate uplift. Section 6 contains the conclusions.

2. THE CASE-STUDY

All LEM simulations in this paper are based on a case of strongly sheared ice clouds, which were observed on 27 December 1999 by the Chilbolton radar (51.145°N, 1.437°W). Hogan and Illingworth (2003) discuss the retrieval of IWC from the radar data. Radiosonde data from Herstmonceux (120 km east, i.e. downwind, of Chilbolton) were used to give temperature and humidity profiles to initialize the LEM. Figure 1 shows radar data from 27 December 1999 and this clearly shows the advection of the fall streaks by the strong wind shear. The radiosonde data (Fig. 2) show that the case contains both high- and low-shear regimes (below/above 7 km) of different stabilities, which are also distinguishable in the radar data (Fig. 1).

3. THE LARGE-EDDY MODEL (LEM)

The effects of shear were investigated using version 2.3 of the LEM (described by Derbyshire *et al.* (1999) and Gray *et al.* (2001)). The LEM is a non-hydrostatic model, which solves an anelastic quasi-Boussinesq set of equations, in either one, two or three dimensions. The model was run with prognostic total water (vapour and liquid), rain and double-moment ice and snow (i.e. prognostic mass and number*). The lateral boundary conditions are periodic, the top is a rigid lid and no fluxes were applied at the surface.

* In this paper 'IWC' and 'IMR' always refers to combined ice and snow, when used to refer to the LEM, except where a clear distinction is made between 'ice' and 'snow'.

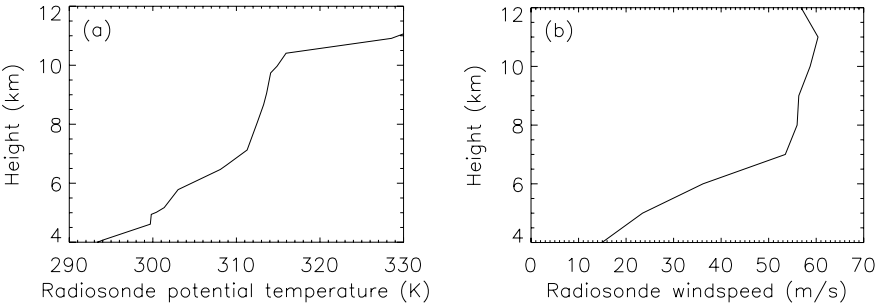

Figure 2. Radiosonde profiles of (a) potential temperature and (b) wind speed at 1100 UTC on 27 December 1999 from Herstmonceux (120 km east of the Chilbolton radar). There is a stable high-shear cloud layer (4.5 to 7 km) and a less stable lower-shear cloud layer (7 to 10.5 km).

Unfortunately, there is no turbulent enhancement of ice fall speeds or collision rates in the LEM, which may be significant for runs with significant turbulence from wind shear and wave breaking (Pinsky and Khain 1998; Shaw 2003).

A large domain of 50 km was used, to minimize the effects of using periodic lateral boundary conditions with high wind speeds; doubling the size of the domain was found to have very little effect on the results. A 100 m horizontal resolution and a vertical resolution of 125 m in the cloud layer were used; this is a much higher resolution than many CRM studies (Xu *et al.* 2002) and is expected to capture the within-cloud circulations of this case (Petch and Gray 2001). Reducing the horizontal resolution to 50 m affected mean ice mixing ratios (IMRs) by less than 20%. Three-dimensional (3D) modelling of this domain with this shear is computationally very expensive, so the model was run in two dimensions. This is not unusual for CRM studies (Starr *et al.* 2000; Xu *et al.* 2002) and both Moeng *et al.* (1996) and Tompkins (2000) showed that 2D simulations can give good results when compared with 3D model runs. However, the effects of using a third dimension in this sheared case is being investigated. Above 11 km, the LEM vertical resolution was reduced and a damping layer applied; this was found to effectively damp gravity waves above the cloud. It was also found to be very important to use a smooth reference potential temperature profile (which is used to calculate buoyancy forces in the LEM), otherwise unnaturally large gravity waves could form at the tropopause when a large shear was applied.

The radiation model from Fu and Liou (1992, 1993), where ice is treated optically as hexagonal shapes, is incorporated into our version of the LEM. In addition, we also used the updated ice of Fu (1996) and Fu *et al.* (1998). The model is a four-stream model and uses six solar and twelve infrared bands. It uses the independent-column approximation, but is still computationally expensive*. Due to the high wind speeds used, this was called every 18 seconds but the results are almost identical if this frequency is increased to every five seconds.

(*a*) *LEM initialization*

As already discussed in section 1, the LEM was initialized by cooling it, at a rate derived from the estimated uplift, to give the observed temperature and humidity profiles, rather than forcing the LEM boundaries with output from a larger-scale model. This avoids running another model and also avoids introducing errors from that model

* A Monte-Carlo radiative transfer scheme has been applied to similar cases within the LEM. These results suggest that the independent-column approximation should introduce small errors in this study.

into the LEM. (There were significant differences between the Unified Model profile and the radiosonde profile in this case.) However, cooling is a significant simplification of the complex process of frontal uplift. A potential temperature profile was constructed so that cooling the cloud layer (i.e. 5 to 10 km, with the cooling decreasing linearly to zero at 1 km and 15 km) at 0.001 K s^{-1} would reproduce the observed profile in two hours if no latent heat release or mixing occurred. This cooling rate was estimated from the observed slope of the cloud base (i.e. equivalent to an uplift of 10 cm s^{-1}). The initial water profile was set to the radiosonde values increased to 1.1 times saturation with respect to ice in the cloud layer (since this gave a IWC profile similar to that observed), and the observed cloud ice was initialized as vapour. Since the latent heat release over the two hours is comparatively small, this method gave a good match (to within 1 K) with the potential temperature profile observed by the radiosonde.

Small initial random perturbations (± 0.1 K and $\pm 5\%$ of the initialized water vapour) were imposed on the first time step to allow inhomogeneities to develop (Starr *et al.* 2000; Dobbie and Jonas 2001). The model was initialized with a wind speed of zero at all model levels. After 400 s, the wind was artificially forced to the observed profile; this forcing affected the horizontally averaged wind at every model level, whilst preserving the horizontal variations from that mean. If the model was initialized with a wind present, the wind affected the field of random perturbations added on the first time step by affecting the numerical diffusion of these small-scale features. This process depended on the magnitude of the wind speed and not the wind shear. This significantly affected the final results, since higher winds tended to smooth perturbations to almost zero in regions where the perturbations were small. This led to a more 'clumped' initial distribution of ice and less convection at upper levels after the model spin-up.

Figure 3(a) shows that the LEM gave a horizontally averaged IMR profile similar to that observed at 1000 or 1030 UTC, although the vertical distribution is too bimodal and the upper peak in the IMR is too large. The radiosonde profile used was from 1100 UTC, but it is not surprising that the LEM does not give the IWC profile observed at that time, since Chilbolton (the radar site) and Herstmonceux (the radiosonde site) are 120 km apart. The lower peak in the IMR profile in the LEM corresponds to a peak in the snow mixing ratio and is located in the lower stable region, which has a high wind shear (Fig. 3(b)). The two upper peaks correspond to peaks in the IMR; these occur in the upper levels which are stable with lower shear. So, the two main peaks correspond to the convecting and fall-streak regions of the cloud, but it seems likely that the discontinuous treatment of ice and snow in the LEM may increase this bimodality of the IMR profile. The magnitude of the IMR in the LEM is similar to that observed, given an error bound on the observations of approximately a factor of two (Hogan and Illingworth 2003).

In Fig. 3(a), the modelled cloud base is too low, but this is expected, given (i) the difference in the positions of the radiosonde and the radar and (ii) that the observed ice was initialized as vapour at the heights at which it was observed, and the ice formed in the LEM falls over the duration of the model spin-up. There is significant uncertainty in fall speeds (Heymsfield and Iaquinta 2000) and, as already noted, no turbulent enhancement of aggregation in the LEM (which may lead to larger particles and larger fall speeds). Figure 3(b) shows that the profile is very sensitive to the fall speeds, but the height of the cloud base is largely unaffected, because the air below the cloud is much dryer than the air in the cloud. Doubling the fall speeds does not halve the IMR within the cloud, but rather decreases the magnitude and height of the highest peak in IMR, whilst the peak in snow mixing ratio is less affected. This leads to a less bimodal distribution. In the future, using Doppler radar data may help constrain uncertainties arising from variations in fall speeds and initializations.

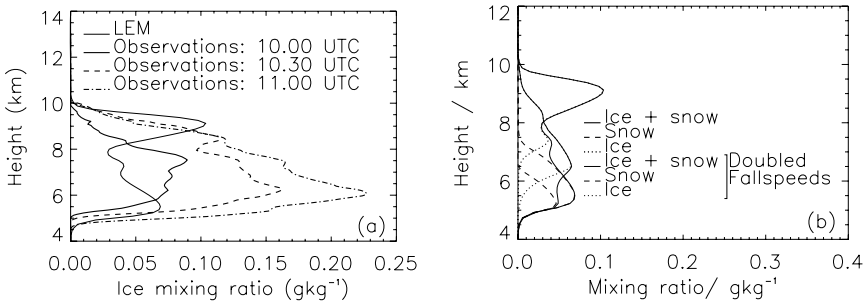

Figure 3. (a) A comparison of the large-eddy model (LEM) ice and snow mixing ratio (IMR) profile (thin solid line) and radar-retrieved profiles from 0945–1015, 1015–1045 and 1045–1115 UTC (bold lines, shown as solid, dashed and dash-dotted respectively). (b) Contributions of ice (dotted lines) and snow (dashed lines) to the total IMR profile (solid lines), with (thin) and without (bold) doubled fall speeds.

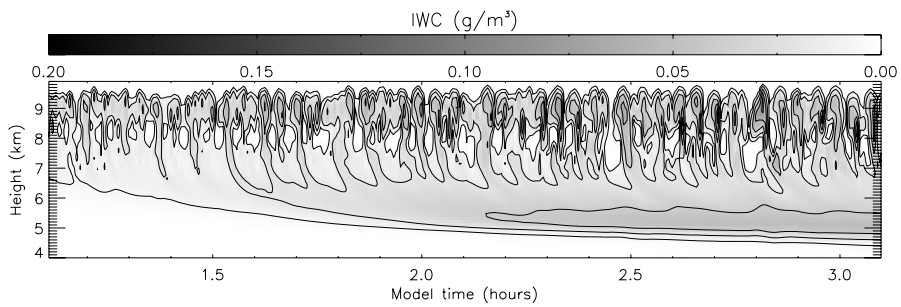

Figure 4. Time–height cross-section of ice water content (IWC) from the large-eddy model. Vertical profiles of IWC were sampled and averaged in time so as to mimic the 94 GHz Chilbolton radar. After two hours of model time, the temperature profile in the model matches the 1100 UTC radiosonde from Herstmonceux.

In this work, we have sought to mimic the observing instrument within the LEM, by simulating the radar scan. Using a fixed time step of one second allowed the mean IWC from 30 one-second intervals to be output from the LEM, thus simulating the sampling of the radar data (ignoring differences caused by the LEM resolution of 100 m and the radar beam width of 80 m at 10 km). This gives a visual comparison between the LEM field (Fig. 4) and the observed field (Fig. 1), though we do not expect exactly the same time evolution in the two cases, because the LEM is not actually simulating the frontal uplift. The LEM is clearly capturing the convective cells above 7 km and the homogenizing effects of the shear below that level, although the cloud below 7 km is more homogeneous in the LEM than in the radar observations.

Simulating the radar data allows us to compare the structure of the IWC field in the LEM with the observations, using spectral analysis. Fourier transforms of the IWC from individual levels of the LEM can be compared with the radar data, using the observed wind speed to convert from time to space, but this approach does not account for the time averaging used in the radar data. In addition, we wanted to compare the structure of the ice water path (IWP) over deeper layers, which have varied wind speeds over their depth. Taking Fourier transforms of the simulated radar data allows us to do this (as well as accounting for the time averaging of the radar). Figure 5 shows Fourier transforms of the IWP in the low- and high-shear layers. (Radar data from 0945 to 1045 UTC were used, since IWC profile in the LEM is similar to that observed at 1015 UTC.)

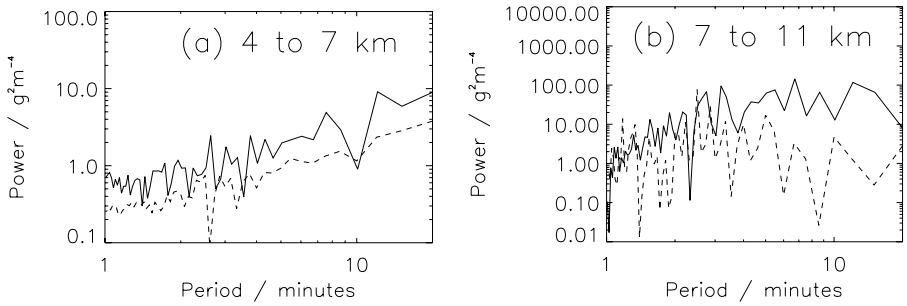

Figure 5. Power spectra of the ice water path from the radar data (0945 to 1045 UTC, solid line) and from the radar simulation within the large-eddy model (from 1.5 to 2.5 hours model time, dashed line), computed from original data shown in Figs. 1 and 4. (a) shows the strongly-sheared lower layer (4 to 7 km, one minute $\simeq$1 to 3 km), and (b) the upper low-shear layer (7 to 10 km, one minute $\simeq$3.5 km).

This shows that the LEM captures the scales of variability well at upper levels. This gives a Fourier transform similar to that observed for features with periods of less than 6 minutes (approximately 14 km), but the larger scales are less well represented. At lower levels (below 7 km), there is less variability in the LEM than in the observations. This is also seen in the p.d.f. of IWC discussed further in section 4(a).

As well as varying fall speeds, sensitivities to the cooling rate and random perturbations were also investigated. Cooling the LEM to the observed profile at one third, or three times, the rate previously applied affected IWC by a factor of approximately two. Changing the magnitude of the random temperature perturbations (by a factor of three), or the random seed used, could change the IWC at some model levels by up to 20%, or 10%, respectively.

This initialization provided an LEM case-study to investigate the effects of wind shear, with a reasonable basis in the observational data. It does not provide a validation of the LEM, by comparing modelled and observed fields, since the observations do not sufficiently constrain the model initialization and the model cloud is not formed by the full complex process of frontal uplift, but rather by an imposed cooling.

4. THE EFFECT OF WIND SHEAR ON THE CIRRUS

The LEM was run with between 0.0 and 1.2 times the observed shear, in order to explore the effects of the wind shear on the cloud. Figure 6 shows that the variation between the runs was small (smaller than the variation introduced by using a different seed for the random number generator used to produce the initial random perturbations i.e. $\simeq$10%). However there is consistently ($\simeq$20%) more ice between 7.5 and 8.0 km in runs with shear; there is also a peak in the observed IMR profiles at this level (Fig. 3). Figure 7 shows that shear tends to increase vertical velocities and TKE densities between 5 and 8 km. (The p.d.f. of the vertical velocities at any level is normally relatively unskewed and mono-modal (not shown).) Shear can lead to very patchy and intermittent Kelvin–Helmholtz wave breaking at the base of the convective cells and this can increase the microphysical production of ice between 7.5 and 8.0 km (not shown). The effect of more extensive Kelvin–Helmholtz wave breaking is investigated in section 5.

Figure 8 shows that shear significantly changes the 2D distribution of ice. With and without shear, we see a region of convective overturning in the less stable low-shear layer above 7 km (driven by long-wave cooling at cloud top and latent heat release in the updraughts). Below this is a region of fall streaks, which are quickly advected relative

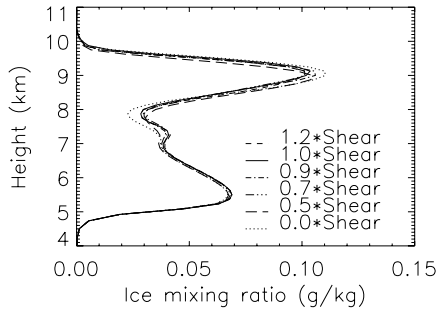

Figure 6. Horizontally averaged profiles of ice mixing ratio from runs with between 0.0 and 1.2 times the observed shear.

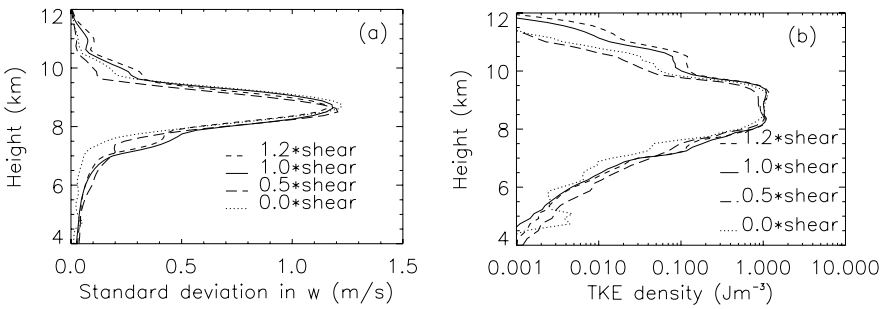

Figure 7. Standard deviation in (a) vertical velocity and (b) turbulent kinetic energy (TKE) density, as a function of height with varying shear. (For clarity, fewer lines are shown than in Fig. 6).

to their source in the convective layer by the shear. The shear also homogenizes the fall streaks, particularly for the more strongly sheared case. The shear leads to asymmetries in the convection and fall streaks but, as we have seen, this has little effect on the mean IWC profile.

It was also noted in the LEM runs that with shear the turbulence was sometimes anisotropic (at scales smaller than 1 km) in the stable layer. Such anisotropic turbulence has been observed in aircraft data from thick frontal cirrus clouds and may occur because of the atmospheric stability suppressing vertical motions (Smith and Jonas 1996). In the LEM, the turbulence was always much more isotropic in the convective layer and anisotropic turbulence was only noted with shear. It seems that the shear is distorting the turbulence, but it is possible that anisotropic turbulence can occur without shear, although this was not noted in this case.

(*a*) *Probability density functions of total water content and IMR*

There is a move towards cloud schemes that use prognostic p.d.f.s to represent the variations in water content within a single GCM grid cell (Tompkins 2002; Wilson and Gregory 2003). Figure 9 shows that a skewed mono-modal distribution (as used by Tompkins 2002 and Wilson and Gregory 2003) provides a good fit for the total water contents in this sheared ice cloud case-study. However, the p.d.f.s from the LEM include variance only from the resolved small-scale circulations (which have developed from the 100 m scale random perturbations added initially), rather than larger-scale processes, which will affect the sub-grid variance in a GCM. The IMRs follow a similar form but, as noted by Tompkins (2002), the assumption of zero supersaturation is invalid for

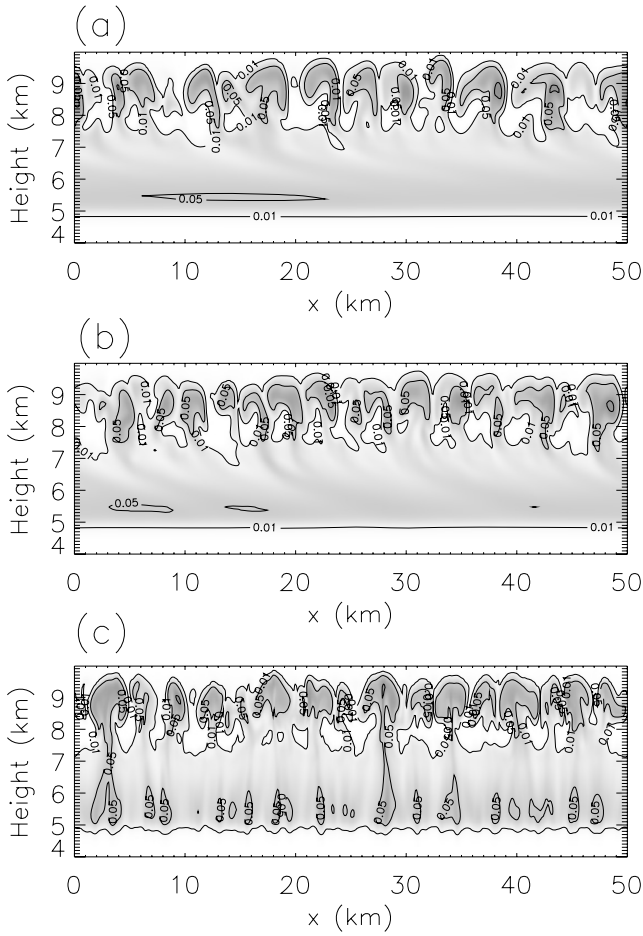

Figure 8. Modelled ice water content fields (g m^{-3}) (a) with shear, (b) with half shear, and (c) with no shear.

many ice clouds (including this case-study, which is significantly supersaturated with respect to ice between 6 and 7 km). Shear-induced mixing has a significant effect on the modelled p.d.f.s at lower levels (5.5 km), whilst in the upper convective region (8.5 km) the p.d.f. is relatively unaffected. At 7.0 km, shear broadens the p.d.f.; this may occur because of increased ice production and sublimation from shear-induced turbulence.

P.d.f.s of IWC from radar data were also compared with the LEM results (radar data from 0945 to 1045 UTC were again used). This was achieved by using p.d.f.s calculated from the simulated radar data, rather than from the LEM spatial domain. This gives the same time averaging as the radar and also includes the variation of the field with time (as observed by the radar) rather than only space (although, as noted previously, we do not expect the time development of the LEM field to exactly match that observed by the radar). Comparing Figs. 9 and 10, we see that the differences between the p.d.f.s derived from the simulated radar data and from the LEM domain are normally small (i.e. the variations over time and the time-averaging effects of the radar sampling have little effect on the p.d.f.s) except at 5.5 km. Here the lowering of the cloud base over time has a significant effect. Figure 10 shows that the essentially monotonically decaying p.d.f. of

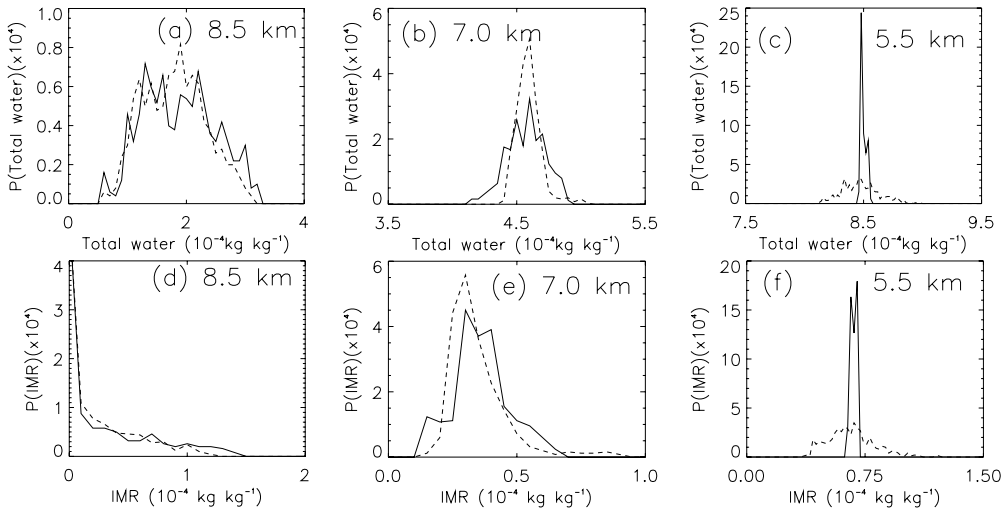

Figure 9. Probability density functions of total water evaluated over the large-eddy model domain at two hours model time at heights of (a) 8.5 km, (b) 7.0 km and (c) 5.5 km, with shear (solid) and without shear (dashed). (d) to (f) are as (a) to (c), but for ice mixing ratio.

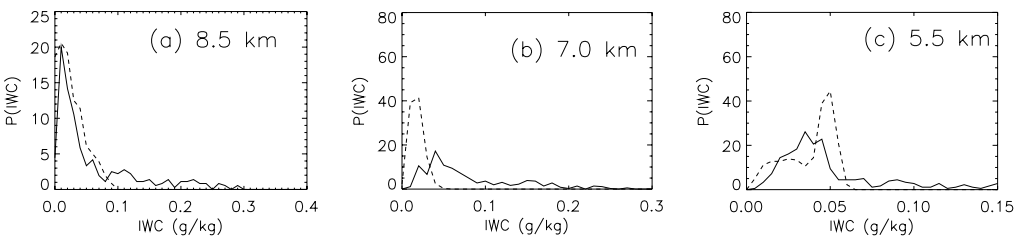

Figure 10. Probability density functions of ice water content from the Chilbolton radar at 0945–1045 UTC (solid line) and from the simulated radar data (dashed line) at 1.5–2.5 hours model time, at heights (a) 8.5 km, (b) 7 km, and (c) 5.5 km.

IMR at 8.5 km matches the observations reasonably well, although the LEM is also not capturing the largest IMRs. Again at 5.5 and 7 km the LEM is not capturing the largest IMRs and at 7 km the IWC in the LEM is too low. At 5.5 km, although the IWC in the LEM is homogeneous, the p.d.f. is broad, because of the change in cloud base over time. The high peak at 0.05 g kg^{-1} is again evidence of a more homogeneous IWC field in the LEM than the observations. So, as noted in the Fourier transforms (Fig. 5), the upper-level structure is showing developed convection, but this is not being preserved as such clearly distinct fall streaks at lower levels. This may be because the largest IWC and larger scales of spatial variability are not being captured by the LEM, or because mixing is too rapid in the lower levels.

Figure 11(a) shows the fractional variance in IWC (i.e. the variance in IWC divided by the mean IWC squared) in the LEM compared with the radar observations. This again highlights that the IWC field in the LEM is more homogeneous than the observations (except at 8 km where regions of low IWC increase the fractional variance). If the larger IWCs are excluded from the variance calculations (Fig. 11(b)), the model and observations are more similar. The LEM is clearly not capturing the largest IWC seen

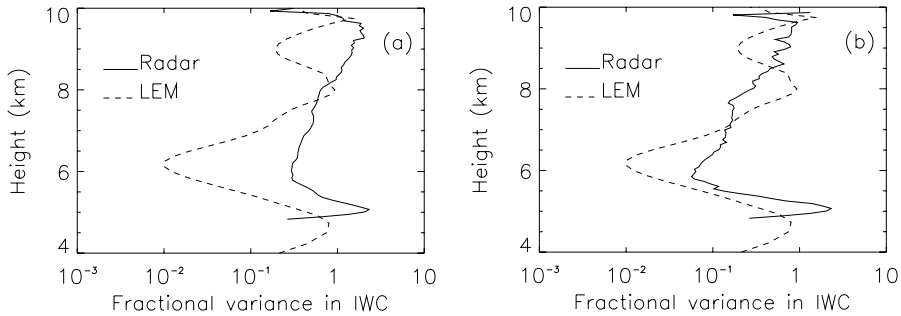

Figure 11. Fractional variance (see text) in ice water content as a function of height in the large-eddy model at 1.5–2.5 hours model time (dashed line) and from the radar (solid line) from 0945 to 1045 UTC. (a) shows statistics for all pixels with detectable ice, and (b) shows statistics for detectable IWC less than 0.1 g m^{-3}.

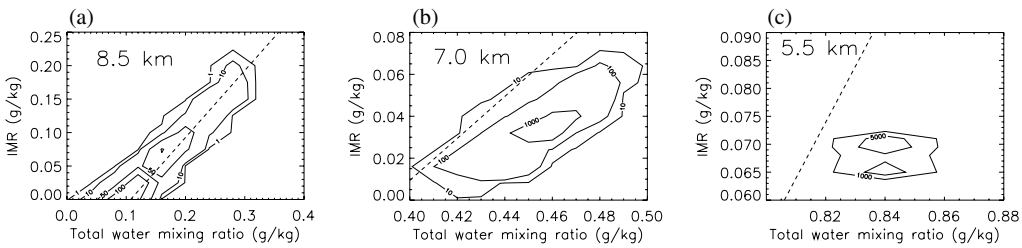

Figure 12. Probability density functions of total water and ice mixing ratio (IMR) at two hours model time at heights (a) 8.5 km, (b) 7 km, and (c) 5.5 km. Dashed lines represent zero supersaturation with respect to ice.

in the radar data at upper levels and this leads to a more homogeneous IWC field in the sheared fall-streak region.

Figure 12 shows the relationship between IMR and total water in the LEM. At 7.0 and 8.5 km, the two are well correlated, since ice is being generated at these levels. There is a greater supersaturation at 7.0 km since this region is too warm for homogeneous nucleation. At 5.5 km there is essentially no correlation between IMR and total water mixing ratio. Ice is still growing by vapour deposition at this level, and without shear the two variables are still correlated (not shown). However, shear-induced mixing reduces this correlation and the variances in the two variables.

(*b*) *Vertical decorrelation of IWC*

Figure 13 shows the mean correlation coefficient between the IWC at different levels as a function of the vertical separation of those levels for (i) the sheared LEM case, (ii) the zero-shear case, and (iii) the radar data (from Hogan and Illingworth 2003). As noted by Hogan and Illingworth (2003) in the sheared case, there seems to be a linear relationship between correlation coefficient and the vertical separation for low separations. Figure 13 shows that this occurs with or without shear, but the gradient decreases with increased shear. The results from Hogan and Illingworth (2003), which do not include the zero-shear case (because they are observational results), agree with the modelled results for the both the high- and low-shear regimes.

After the initial linear regime, the correlation coefficient is positive without shear, even for separations as large as 3.5 km. With shear, there are oscillations in the correlation coefficient about a value of approximately zero. These oscillations occur because

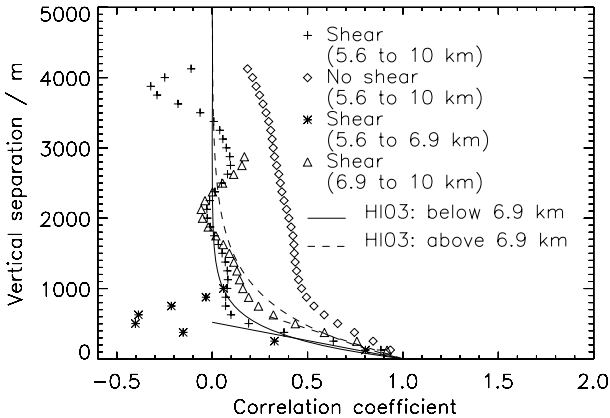

Figure 13. Decorrelation of ice water content with height. Symbols show the large-eddy model data: with shear (+) and without shear (◇) from 5.6 to 10.0 km, and for the high-shear (5.6–7 km, ∗) and low-shear (7.0–10.0 km, △) regions only. The solid and dashed lines are fitted to the radar data from Hogan and Illingworth (2003) (HI03) for high-shear (4.9–6.9 km) and low-shear (6.9–8.9 km) regions.

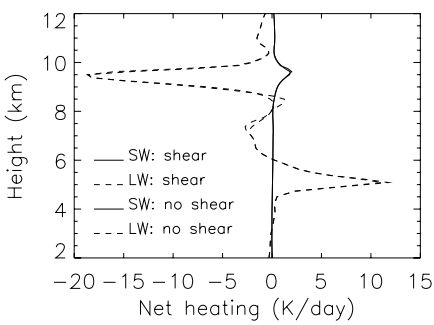

Figure 14. Modelled short-wave (SW) and long-wave (LW) horizontally averaged radiative heating rates.

of the sheared fall streaks; the correlation coefficient increases as a neighbouring streak (gap) is advected over a lower streak (gap). Although these oscillations have little effect on the mean radiative transfer in this case, they may be more significant in cases of partial cloud cover. The relationship between the correlation coefficient and vertical separation is similar to that noted by Hogan and Illingworth (2000) for the cloud-overlap parameter and vertical separation, suggesting that this relationship may also be strongly shear dependent, at least for small separations.

(*c*) *Radiation*

Varying the radiation used (both long-wave and short-wave, long-wave only, short-wave only, and no radiation) shows that the convective cells above 7 km are driven mainly by long-wave cooling at the cloud top. The short-wave radiation reduces the mean IMR profile by less than 10% and has little effect on the cloud structure, because the solar elevation is so low in southern England in December ($\simeq$14° at 1100 UTC). Figure 14 shows how the shear has little effect on the heating rates within the cloud, the differences in the long-wave heating rate just reflecting the small difference in IMR profile (Fig. 3). Shear only affects surface and top-of-atmosphere (TOA) fluxes

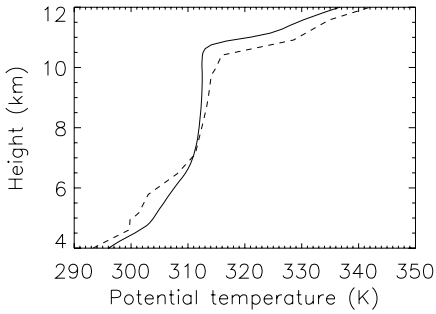

Figure 15. Potential temperature profile from the radiosonde (dashed line) and for the runs initialized with a less stable profile (solid line). Richardson numbers are less than 0.25 for runs with ≥0.9 times the observed shear.

by up to 0.5 W m^{-2}. Much larger differences would be expected for a case with fractional cloud cover. In this case the relative advection of ice by the wind shear would significantly increase the fraction of the sky covered by cloud. This affects solar and long-wave fluxes differently depending on the optical thickness of the cloud (Hogan and Kew 2004).

5. Effects of critical Richardson numbers

This section describes a modified case-study which gave more extensive Kelvin–Helmholtz wave breaking. In this case, we study wave breaking effects both with and without large-scale uplift.

The case-study was modified, by reducing the atmospheric stability, in order to give more extensive Kelvin–Helmholtz wave breaking for large shears (Fig. 15). Such wave breaking was observed by Smith and Jonas (1996) in frontal cirrus. We expect wave breaking to occur when the gradient Richardson number is below 0.25 (Turner 1973). The gradient Richardson number, *Ri*, is defined by

$$Ri = \frac{N^2}{\left\{\left(\frac{\delta u}{\delta z}\right)^2 + \left(\frac{\delta v}{\delta z}\right)^2\right\}}, \tag{1}$$

where u and v are the horizontal wind velocities, z is height and N is the Brunt–Väisälä frequency,

$$N^2 = \frac{g}{\theta_v}\frac{\delta\theta_v}{\delta z} \tag{2}$$

(g is the acceleration due to gravity and θ_v is the virtual potential temperature).

(*a*) *Effects with large-scale uplift*

Various shears were applied to the cloud, and significant areas with Richardson numbers below 0.25 occurred in the shear layer for runs with shear ≥0.9 times the observed shear. Figure 16 shows contours of Richardson number superimposed on a grey-scale image of IWC. For runs with less than or equal to the observed shear, the IWC field looks fairly similar to the previous case. With 1.2 times the observed shear, there is Kelvin–Helmholtz wave breaking across almost the entire domain and this

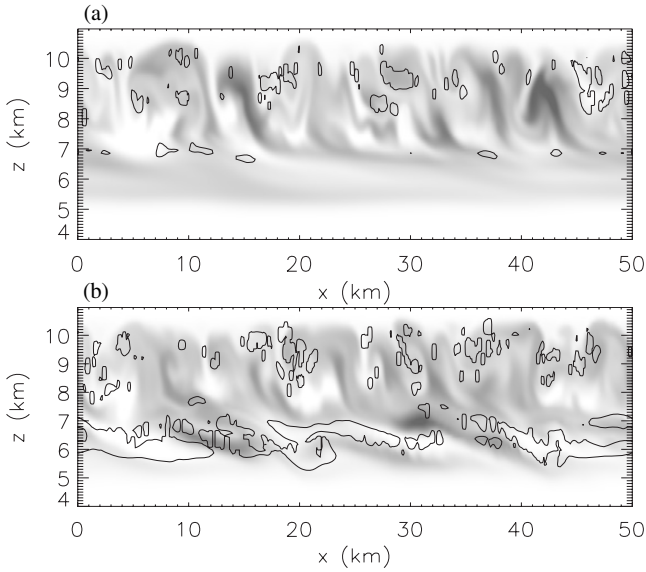

Figure 16. Contours of Richardson number, $Ri = 0.25$, (smoothed over 3×3 grid boxes) superimposed on a grey-scale image of ice water content for (a) 1.0 and (b) 1.2 times the observed shear. We expect wave breaking inside the contour.

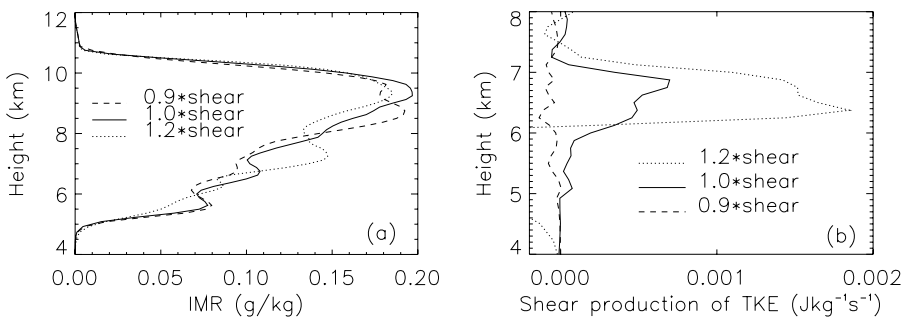

Figure 17. Effects of varying the shear on (a) the horizontally averaged ice mixing ratio profile, and (b) the shear production of turbulent kinetic energy, for a cloud formed by cooling to simulate uplift.

dominates the cloud structure in the shear layer. The profile of IMR is significantly affected (Fig. 17(a)).

The wave breaking completely alters the TKE production by shear. Figure 17(b) shows that increasing the observed shear to 1.2 times that observed affects the shear production of TKE by a factor of approximately three. (As noted in section 3, the full effects of this on fall speeds and collision rates are not captured in the LEM.) This leads to increased microphysical generation of ice in the shear layer (Fig. 18). In particular, Fig. 18 shows that wave breaking gives nucleation where it does not otherwise occur, and extensive wave breaking doubles the deposition and sublimation rates.

These effects result in changes in the surface and TOA fluxes of up to 2% or 0.5 W m^{-2} compared with the zero-shear case (Table 1) and the fluxes typically differ from the 0.7 shear case (i.e. a sheared case with very little Kelvin–Helmholtz wave breaking) by 0.25 W m^{-2}.

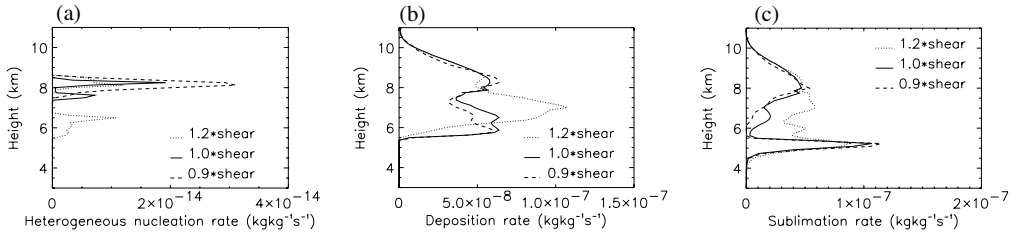

Figure 18. Effect on modelled (a) heterogeneous nucleation, (b) deposition, and (c) sublimation rates of extensive Kelvin–Helmholtz wave breaking (with 1.2 times the observed shear, dotted line), of limited wave breaking (1.0 times the observed shear, dotted line) and of little wave breaking (0.9 times observed shear, dashed line). Wave breaking has significant effects on all three processes.

TABLE 1. SHEAR-INDUCED CHANGES (COMPARED WITH THE ZERO-SHEAR CASE) IN MEAN TOP-OF-ATMOSPHERE (TOA) AND SURFACE FLUXES

		1.2 × shear		0.7 × shear	
		%	W m^{-2}	%	W m^{-2}
Short-wave flux	upwards (TOA)	−0.17	−0.49	−0.10	−0.30
	downwards (surface)	1.55	0.49	0.75	0.24
Long-wave flux	upwards (TOA)	0.30	0.31	0.54	0.55
	downwards (surface)	0.52	1.60	0.44	1.40

Shear at 1.2 (0.7) times the observed shear implies conditions with (without) Kelvin–Helmholtz wave breaking.

Section 4 showed effects of very limited turbulence from localized areas with $Ri < 0.25$. In this second modified study with 1.0 times the observed shear, the regions with $Ri < 0.25$ are again localized ($\simeq$250 m deep and 2 km across) (Fig. 16) and again have a significant effect on microphysical processes (Fig. 18). This thin layer, with $Ri < 0.25$, is hardly resolved if the LEM's vertical resolution is doubled to 250 m. The layer is certainly much smaller than would be resolved by a GCM (typically 300 m vertical resolution and 20 km horizontal resolution) and such effects are not currently parametrized in most GCMs. Plotting the range of Ri against mean Ri showed that we can expect some wave breaking when the horizontally averaged Ri is less than 0.5 (not shown). In reality, we also expect background gravity-wave activity to interfere sometimes with other motions to give Kelvin–Helmholtz wave breaking where it would not otherwise occur (Smith and Jonas 1996). This effect was not investigated in this study, but the significant effects of wave breaking on the cloud suggests that it merits future work.

(*b*) *Shear effects without large-scale uplift*

Further runs were performed with no imposed cooling (i.e. no simulated uplift) to isolate the effects of wave breaking on cloud formation. The initial water vapour mixing ratio was set to 1.2 times the saturation mixing ratio between 5 and 10 km and the radiosonde values were used elsewhere. Small random perturbations were again applied between 6 and 10.5 km to allow cloud inhomogeneity to develop. The wind speed was set to zero initially and gradually increased to 1.2 times that observed in one run and set to zero in the other.

As expected, the strong shear gave Kelvin–Helmholtz breaking and this has a very significant effect on the mean IMR profile (Fig. 19). The wave breaking gives a cloud layer at 5 to 8 km that does not otherwise occur, and this contains sufficient

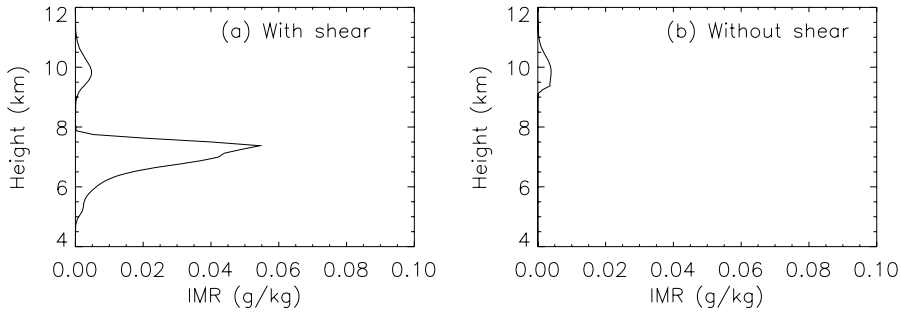

Figure 19. Ice mixing ratio profiles (a) with shear and (b) without shear.

ice ($\simeq$0.05 g kg^{-1}) to have a significant impact on TOA radiative fluxes. (The cloud decreases the upward infrared flux by 53 W m^{-2}, or 23%, and increases the upward solar flux by 0.14 W m^{-2}, or 33%.) Without the wave breaking, the vertical velocities induced by the radiative forcing and latent heat release are insufficient to form a cloud at these lower levels. At low and middle latitudes, the upper atmosphere is frequently saturated with respect to ice, but not cloudy (Jensen *et al.* 2001), and these results suggest that, where other large-scale forcings do not exist, the vertical velocities generated by Kelvin–Helmholtz wave breaking can have very significant effects on cirrus cloud formation and maintenance. However, investigations of these effects were not pursued further, because future work is planned using observational data from a case.

6. Conclusions

This paper has investigated the modelled effects of wind shear on an LEM case-study, which was based on a radiosonde profile and data from the Chilbolton radar (Hogan and Illingworth 2003). Cooling the LEM to the observed profile gave an ice mixing ratio in reasonable agreement to that observed, without tuning the run to the observations (except by setting the water vapour mixing ratio to 1.1 times the saturation value, in order to give large enough IWC at the end of the model spin-up time). The IMR profile was more bimodal than the observations and this appears to be related to the discontinuous representation of ice and snow in the LEM.

Varying the shear applied in the LEM allowed the effects of shear on this case to be investigated. Shear advected the fall streaks away from their source and increased mixing, but otherwise had little effect on the cloud, unless Kelvin–Helmholtz wave breaking occurred. In this case-study, wave breaking was limited and was found to occur in small patches when the horizontally averaged gradient Richardson number was less than 0.5. As a result, the shear had little effect on the radiative heating rates within the cloud, or the surface or TOA fluxes. However, these fluxes would be significantly affected for a more patchy cirrus cloud where the shear would increase the cloud area fraction (Hogan and Kew 2004). These results support the assumption that, when extensive Kelvin–Helmholtz wave breaking does not occur, advection is the most important effect of shear for radiative transfer (Hogan and Kew 2004), with shear-induced mixing as a secondary effect. However, it should be noted that the effects of strong shears on the upper convective region of the cloud were not investigated. In contrast to the small effects of wind shear in this case, the IWC profile was very sensitive to the fall speeds used and doubling the fall speeds reduced upper-level ice significantly. Unfortunately Doppler radar data were not available for comparison with the LEM for this case.

In the low-shear region (below 7 km), the spatial variability was similar to that observed at scales less than ≈14 km, whilst the cloud was more homogeneous at lower levels (section 3(a)). P.d.f.s of IWC were similar to those observed, although the largest IWCs were not captured and there was insufficient variability in the lower fall-streak region. Similarly, the LEM captured the fractional variance in IWC best at upper levels, especially if the largest IWCs were removed from the observations, but there was too little variance at lower levels. Since the LEM is not capturing the largest IWCs and largest spatial scales of variability, this seems to lead to a lack of inhomogeneity in the fall-streak region, although it is possible that there is also too much mixing in the model. P.d.f.s of both IMR and total water were well fitted by skewed mono-modal distributions (as used in new statistical prognostic cloud parametrizations, section 4(a)). However, significant supersaturations with respect to ice were maintained in the LEM, and shear decreased the correlation between total water and ice water mixing ratios.

The relationship between the correlation of IWC at different levels and the separation of those levels is shear dependent and initially linear, with or without shear, and this gradient depends on the shear. Shear can also cause oscillations in this correlation coefficient as streaks are advected over gaps, or gaps over streaks (section 4(b)).

Modified case-studies showed that shear effects are case sensitive. In section 5, the atmospheric stability was slightly decreased and this gave much more extensive Kelvin–Helmholtz wave breaking. Wave breaking increased vertical velocities and so significantly affected microphysical processes, in particular giving nucleation where it did not otherwise occur. This resulted in a significant changes in the IWC profile. The wave breaking would often not be captured at poorer resolutions, because it occurs in thin layers, which have limited horizontal extent (although sometimes these small-scale effects could possibly be aliased to larger scales at coarser resolutions).

Model runs with no imposed large-scale cooling suggested that shear effects are most significant when other cloud-generating mechanisms are weaker, i.e. without the strong frontal uplift. In such cases, shear-induced turbulence can allow significant cloud to form, when it does not do so otherwise. (This affected TOA fluxes by up to 53 W m^{-2}.) Studying observational data from such a case would give a better understanding of these processes and some indication of how frequently this occurs in the atmosphere.

Finally, although this study does not give a validation of the LEM against observations (because the LEM is not sufficiently constrained), it has demonstrated the benefits of combining LEM modelling and radar data, i.e. the radar is able to give 2D data of a sufficiently high resolution and the LEM allows many unobservable variables to be studied and forcings to be varied.

ACKNOWLEDGEMENTS

We would like to thank Robin Hogan, University of Reading, UK for providing the radar data, Sat Ghosh and Doug Parker from the University of Leeds for interesting discussions and advice and also Sat Ghosh for proofreading. We would also like to thank both anonymous reviewers for their constructive comments, which have helped to improve both the content and presentation of the paper (in particular the comments made by one reviewer that led us to investigate the effect of the magnitude of the wind on the random perturbations applied in the model spin-up phase). This work was funded by the Natural Environment Research council under NER/M/S/2002/00127 and NER/T/S/2000/00983.

REFERENCES

Barker, H. W. 1996 A parameterization for computing grid-averaged solar fluxes for inhomogeneous marine boundary layer clouds. Part I: Methodology and homogeneous biases. *J. Atmos. Sci.*, **53,** 2289–2303

Benedetti, A. and Stephens, G. L. 2001 Characterization of errors in cirrus simulations from a cloud resolving model for application in ice water content retrievals. *Atmos. Res.*, **59–60,** 393–417

Brown, P. R. A. and Heymsfield, A. J. 2001 The microphysical properties of convective anvil cirrus: A comparison of models and observations. *Q. J. R. Meteorol. Soc.*, **127,** 1535–1550

Buschmann, N., McFarquar, G. M. and Heymsfield, A. J. 2002 Effects of observed horizontal inhomogeneities within cirrus clouds on solar radiative transfer. *J. Geophys. Res.*, **107,** doi: 10.1029/2001JD001273

Cheng, W. Y. Y., Wu, T. and Cotton, W. R. 2001 Large-eddy simulation of the 26 November 1991 FIRE II cirrus case. *J. Atmos. Sci.*, **58,** 1017–1034

Derbyshire, S. H. and Brown, A. R. and Lock, A. P. 1999 'The Meteorological Office large-eddy simulation model'. Turbulence and Diffusion Note 213, Met Office, Exeter, UK

Dmitriev, V. K., Kapitanova, T. P., Pinus, N. G. Potertikova, G. A. and Shur, G. N. 1984 'Mean and microscale structure of wind and temperature fields in jet stream cirrus'. Pp. 347–350 in Vol. II of Proceedings of the 9th International Cloud Physics Conference, Tallinn, Estonian SSR, USSR.

Dobbie, S. and Jonas, P. 2001 Radiative influences on the structure and lifetime of cirrus clouds. *Q. J. R. Meteorol. Soc.*, **127,** 2663–2682

Fu, Q. 1996 An accurate parameterization of the solar radiative properties of cirrus clouds for climate models. *J. Climate*, **9,** 2058–2082

Fu, Q. and Liou, K. N. 1992 On the correlated *k*-distribution method for radiative transfer in nonhomogeneous atmospheres. *J. Atmos. Sci.*, **49,** 2139–2156

1993 Parameterization of the radiative properties of cirrus clouds. *J. Atmos. Sci.*, **50,** 2008–2025

Fu, Q., Yang, P. and Sun, W. B. 1998 An accurate parameterization of the infrared radiative properties of cirrus clouds for climate models. *J. Climate*, **11,** 2223–2237

Gray, M. E. B., Petch, J., Derbyshire, S. H., Brown, A. R., Lock, A. P. and Swann, H. A. 2001 'Version 2.3 of the Met Office large-eddy model'. Turbulence and Diffusion Notes 275–277, Met Office, Exeter, UK

Gu, Y. and Liou, K. N. 2000 Interactions of radiation, microphysics and turbulence in the evolution of cirrus clouds. *J. Atmos. Sci.*, **57,** 2463–2479

Heymsfield, A. J. and Iaquinta, J. 2000 Cirrus crystal terminal velocities. *J. Atmos. Sci.*, **57,** 916–938

Hogan, R. J. and Illingworth, A. J. 2000 Deriving cloud overlap statistics from radar. *Q. J. R. Meteorol. Soc.*, **126,** 2903–2909

2003 Parameterizing ice cloud inhomogeneity and the overlap of inhomogeneities using cloud radar data. *J. Atmos. Sci.*, **60,** 756–767

Hogan, R. J. and Kew, S. F. 2004 'A 3D stochastic cloud model for investigating the radiative properties of inhomogeneous cirrus clouds'. Pp. 1669–1672 in the Proceedings of the 14th International Conference on Clouds and Precipitation, Bologna, Italy

Jensen, E. J., Toon, O. B., Vay, S. A., Ovarlez, J., May, R., Bui, P., Twohy, C. H., Gandrud, B., Pueschel, R. F. and Schumann, U. 2001 Prevalence of ice-supersaturated regions in the upper troposphere: Implications for optically thin ice cloud formation. *J. Geophys. Res.*, **106,** 17253–17266

Larson, V. E., Wood, R., Field, P. R., Golaz, J., Vonder Haar, T. H. and Cotton, W. 2001 Systematic biases in the microphysics and thermodynamics of numerical models that ignore subgrid-scale variability. *J. Atmos. Sci.*, **58,** 1117–1128

Li, J., Dobbie, S., Räisänen, P. and Min, Q. 2005 Accounting for unresolved clouds in a 1D solar radiative transfer model. *Q. J. R. Meteorol. Soc.*, **131,** 1607–1630

Liou, K. N. and Rao, N. 1996 Radiative transfer in cirrus clouds: Part IV: On cloud geometry, inhomogeneity and absorption. *J. Atmos. Sci.*, **53,** 3046–3065

Liu, H. C., Wang, P. K. and Schlesinger, R. E. 2003 A numerical study of cirrus clouds. Part I: Model description. *J. Atmos. Sci.*, **60,** 1075–1084

Luo, Y. L., Krueger, S. K., Mace, G. G. and Xu, K. M. 2003 Cirrus cloud properties from a cloud-resolving model simulation compared to cloud radar observations. *J. Atmos. Sci.*, **60,** 510–525

Lynch, D. K., Sassen, K., Starr, D. O'C. and Stephens, G. (Eds.) 2002 *Cirrus.* Oxford University Press, New York

Moeng, C. H., Cotton, W. R., Bretherton, C., Chlond, A., Khairoutdinov, M., Krueger, S., Lewellen, W. S., MacVean, M. K., Pasquier, J. R. M., Rand, H. A., Siebesma, A. P., Stevens, B. and Sykes, R. I. 1996 Simulation of a stratocumulus-topped planetary boundary layer: Intercomparison among different numerical codes. *Bull. Am. Meteorol. Soc.*, **77,** 261–278

Petch, J. C. and Gray, M. E. B. 2001 Sensitivity studies using a cloud-resolving model simulation of the tropical west Pacific. *Q. J. R. Meteorol. Soc.*, **123,** 2287–2306

Pinsky, M. B. and Khain, A. P. 1998 Some effects of cloud turbulence on water-ice and ice-ice collisions. *Atmos. Res.*, **47–48,** 69–86

Quante, M. and Brown, P. R. A. 1992 'Turbulence characteristics of different types of cirrus clouds'. Pp. 510–513 in the Proceedings of the 11th International Conference on Clouds and Precipitation, Montreal, Canada

Shaw, R. A. 2003 Particle-turbulence interactions in atmospheric clouds. *Ann. Rev. Fluid Mech.*, **35,** 183–227

Smith, S. A. and Jonas, P. R. 1996 Observations of turbulence in cirrus clouds. *Atmos. Res.*, **43,** 1–29

Starr, D. O'C., Benedetti, A., Boehm, M., Brown, P. A., Gierens, K. M., Girard, E., Giruad, V., Jakob, C., Jensen, E. A, Khvorostyanov, V., Koehler, M., Lare, A., Li, R., Maruyama, K., Montero, M., Tao, W., Wang, Y. and Wilson, D. 2000 'Comparison of cirrus cloud models: A project of the GEWEX cloud systems study (GCSS) working group on cirrus cloud systems'. Pp. 1–4 in Vol. I of the Proceedings of the 13th International conference on Clouds and Precipitation, Reno, Nevada, USA

Tompkins, A. M. 2000 The impact of dimensionality on long-term cloud-resolving model simulations. *Mon. Weather Rev.*, **128,** 1521–1535

2002 A prognostic parameterization for the subgrid variability of water vapour and clouds in large-scale models and its use to diagnose cloud cover. *J. Atmos. Sci.*, **59,** 1917–1942

Turner, J. S. 1973 *Buoyancy effects in fluids.* Cambridge University Press

Wilson, D. and Gregory, D. 2003 The behaviour of large-scale model cloud schemes under idealized forcing scenarios. *Q. J. R. Meteorol. Soc.*, **129,** 967–986

Xu, K. M., Cederwall, R. T., Donner, L. J., Grabowski, W. W., Guichard, F., Johnson, D. E., Khairoutdinov, M., Krueger, S. K., Petch, J. C., Randall, D. A., Seman, C. J., Tao, W. K., Wang, D. H., Xie, S. C., Yio, J. J. and Zhang, M. H. 2002 An intercomparison of cloud-resolving models with the atmospheric radiation measurement summer 1997 intensive observation period data. *Q. J. R. Meteorol. Soc.*, **128,** 593–624